

# Numerical analysis of the deep soil failure mechanism for perimeter pile groups

Michael Watford<sup>1</sup>, Jack Templeman<sup>1</sup>, Zhandos Orazalin<sup>1</sup>, Hang Zhou<sup>2</sup>, Andrea Franza<sup>3</sup>,  
Brian Sheil<sup>1\*</sup>

*<sup>1</sup>Department of Engineering Science, University of Oxford, Parks Road, Oxford, OX1 3PJ, UK.*

*<sup>2</sup>School of Civil Engineering, Laboratory of New Technology for Construction of Cities in Mountain Area, Chongqing University, Chongqing, China.*

*<sup>3</sup>Department of Civil and Architectural Engineering, Aarhus University, Navitas, Inge Lehmanns Gade 10, 8000 Aarhus C, Denmark.*

*\*Corresponding author. Email: [brian.sheil@eng.ox.ac.uk](mailto:brian.sheil@eng.ox.ac.uk). Tel.: 01865274170*

## 1    **ABSTRACT**

2    In this paper, the lateral limiting pressure offered by the deep ‘flow-around’ soil failure  
3    mechanism for perimeter (ring) pile groups in undrained soil is explored using  
4    two-dimensional finite element modelling. A parametric study investigates the role of group  
5    configuration, pile–soil adhesion, group size, pile spacing and load direction on group  
6    capacity and corresponding soil failure mechanisms. The finite element output show that the  
7    plan group configuration (square or circular) has a negligible influence on lateral capacity for  
8    closely spaced perimeter pile groups. When compared to ‘full’ square pile groups with the  
9    same number of piles, the present results suggest that for practical pile spacing ( $\geq$  two pile  
10    diameters), perimeter groups do not necessarily increase capacity efficiency, particularly if  
11    the piles are smooth. Nevertheless, perimeter groups are shown to be characterized by both  
12    the invariance of their capacity to the direction of loading and their highly uniform load-  
13    sharing between piles, which are beneficial features to optimize design.

## INTRODUCTION

Interaction effects between closely spaced pile foundations have been a popular topic in geotechnical literature since the late 1960s, largely due to their detrimental influence on foundation capacity and serviceability (Sheil & McCabe 2015). Approaches for dealing with this phenomenon for vertically loaded pile groups are straightforward to implement, applicable to large ‘non-standard’ groups and demonstrate good predictability (Wang et al. 2016, Sheil et al. 2019). While a large body of research has been conducted on the behaviour of laterally loaded pile groups (e.g. Brown et al. 1987, Rao et al. 1998, Ilyas et al. 2004, Rollins et al. 2006, Comodromos & Papadopoulou 2012, 2013, Fayyazi et al. 2014), design calculations for lateral capacity remain less advanced.

The limiting lateral pressure that a cohesive soil can exert on a laterally loaded pile increases with depth before reaching a constant value below a ‘critical depth’  $z_c$  (Murff & Hamilton 1993). For ‘super-long’ piles, the lateral pile capacity is dominated by the ‘deep failure condition’ i.e. the soil failure mechanism below  $z_c$  (Yao et al. 2012, Liu et al. 2021). For short piles, accurate estimates of this limiting pressure is also a prerequisite for the development of more complete design curves describing the variation in capacity over the pile’s length. The deep failure mechanism for a single pile has been analysed extensively in the literature as a plane strain problem, e.g. Martin & Randolph (2006). Using 3D finite element (FE) analysis Georgiadis (2014) showed that the deep failure mechanism for an infinitely long pile row also corresponds to a 2-D ‘flow-around’ mechanism; this prompted more recent extensions to two side-by-side piles (Georgiadis et al. 2013a, 2013b), tripod groups (Zhao et al. 2017a), tetrapod groups (Zhao et al. 2017b), square groups (Sheil 2021) and rectangular groups (Swallow & Sheil 2021). Application in engineering practice involves incorporating these limiting pressures within existing design methods capable of describing the overall load-displacement of the group, such as those proposed by Comodromos and Pitilakis (2005) and

Comodromos and Papadopoulou (2012, 2013). Alternatively, they may be used as ‘standalone’  $p$ -multipliers to replace empirical values (e.g. AASHTO (2012) and FEMA (2012)) to modify existing  $p$ - $y$  formulations e.g. Brown and Shie (1991), Kallehave et al. (2012), Dash et al. (2017), Zhang and Anderson (2017).

The aim of this paper is to explore the influence of pile group configuration on the lateral soil resistance provided by the deep failure mechanism in undrained soil. In particular, the capacity of perimeter (ring) pile groups and the benefits of relocating inner group piles to the periphery is studied using two-dimensional plane strain analyses. The variables considered in the modelling include the group configuration (i.e. a square or circular ring of piles), group size, loading direction, pile spacing and pile–soil adhesion.

## FINITE ELEMENT MODELLING

### *Geometry and material parameters*

Figure 1 and Table 1 outline the scenarios considered in this FE study (using the software package Abaqus 2019). Perimeter pile groups are arranged in either a square or circular configuration of  $n = 8, 12$  and  $16$  piles. A fixed pile diameter,  $D$ , of  $1$  m and variable pile centre-to-centre spacing,  $s$ , are analysed. While values of  $s/D$  of between  $\sim 2$  and  $\sim 7$  are most common in practice (Mandolini and Viggiani 1997; Sheil and McCabe 2014, 2015),  $s/D < 2$  is also considered in the interest of completeness. Lateral capacity is estimated by applying equal displacements,  $\delta$ , to all piles in the direction  $\theta$ , as shown in Fig. 1. The soil was modelled as a weightless elastic–plastic von Mises material with an undrained shear strength,  $s_u$ , Poisson’s ratio,  $\nu_u = 0.495$  and Young’s modulus,  $E_u = 500s_u$ . The circular pile cross-sections are assumed rigid. The undrained shear strength of the pile-soil interface is  $\alpha s_u$  where  $\alpha$  is the pile-soil adhesion factor, with  $\alpha = 0$  and  $1$  denoting a ‘perfectly-smooth’ and ‘-rough’

interface respectively; this was achieved using the built-in surface-based contact with “rough” ( $\alpha=1$ ) and “frictionless” ( $\alpha=0$ ) formulations.

### *Finite element mesh*

The soil was modelled using six-node quadratic plane strain triangular elements (CPE6H). To achieve rigid bodies, each pile was treated as a separate entity meshed with two-node 2D linear rigid link elements (R2D2) tied to a pile-specific reference node. The pile geometry was modelled as a  $k$ -sided polygon which inscribes the ‘true’ circular pile shape;  $k = 100$  was found to provide an optimal balance between accuracy and calculation time (e.g. Kong (2015)). Pile-soil interaction was modelled using a finite-sliding formulation tangentially to the pile, with full tension strength to prevent pile-soil separation. In all analyses a computational domain size of  $80D \times 80D$  was adopted to ensure all soil failure mechanisms were comfortably contained. All boundaries were restricted from movement normal to their respective surface.

### *Adaptive remeshing*

The FE calculations in this study were performed using an adaptive mesh refinement process which seeks to equalise the quantity  $\int \dot{\gamma}_{\max} dA_e$  over all elements in the mesh, where  $\dot{\gamma}_{\max}$  is the maximum shear strain rate and  $A_e$  is the element area (see Martin (2011)). The element areas are refined by comparing this quantity for each element with the average value for the entire mesh. A schematic illustration of the iterative remeshing process is presented in Fig. 2 which uses Matlab programming to link the open source mesh generator Triangle (Shewchuk, 1996, 2002) with Abaqus. Three remeshing iterations was found to provide a good balance between accuracy and computational efficiency.

87

## 88 *Model validation*

89 A validation was carried out for both a perfectly-smooth and -rough pile-soil interface by  
90 comparing present FE calculations with analytical solutions for a single pile (Randolph &  
91 Houlsby 1984, Martin & Randolph 2006) and FE results for a 3×3 square pile group (Sheil  
92 2021) in Table 2 and Fig. 3, respectively. In this paper, the lateral soil reaction is presented in  
93 terms of the dimensionless capacity factor  $N_s = P/s_u D$  (for a single pile) or  $N_g = P/s_u Dn$  (for a  
94 pile group), where  $P$  is the total foundation horizontal reaction per unit length. In all  
95 validation cases there is excellent agreement, thus confirming the reliability of the developed  
96 modelling procedure.

97

## 98 **NUMERICAL RESULTS**

### 99 *Influence of group geometry*

100 Figure 4 presents the influence of group geometry on  $N_g$  for  $\alpha = 0$  (Fig. 4(a)) and  $\alpha = 1$   
101 (Fig. 4(b)). For  $\alpha = 0$ , the group configuration has a negligible influence on  $N_g$  for closely  
102 spaced piles, ( $s/D \leq 1.5$ ). Interestingly, for  $s/D > 1.5$ , a circular configuration results in a  
103 notable reduction in  $N_g$  and an increase in the spacing required to achieve  $N_g = N_s$ . The  
104 influence of the group configuration on  $N_g$  shows similar trends when the  $\alpha = 1$  condition is  
105 considered (compare Figs. 4(a) and (b)), though the spacing required to reach the asymptotic  
106 value  $N_s$  is now significantly greater than that observed for  $\alpha = 0$ .

107 To further explore the role of the perimeter configuration, FE meshes are presented in Fig. 5  
108 for  $n = 8$  and 16 groups with varied spacing; in this figure, the mesh refinement reflects soil  
109 failure mechanism formation. For brevity, only results for  $\alpha = 0$  are reported. For  $s/D = 2$ ,  
110 both the square and circular groups exhibit ‘block’ failure mechanisms with global flow-

around, regardless of  $n$ ; this explains the similar capacity values observed in Fig. 4 at low values of  $s/D$ . Figure 5 shows that the increase in spacing to  $s/D = 3$  causes different failure mechanisms for the two group configurations: the square group exhibits a hybrid mechanism comprising global flow-around and local interactions between piles, whereas the circular group exhibits local interactions only. At  $s/D = 4$ , soil yielding is confined to between neighbouring piles and therefore the group periphery. This causes a transition from ‘block’ to ‘perimetral’ failure with increasing  $s/D$ . These results clarify that the slight reduction in the values of  $N_g$  observed for the circular groups (compared to the square groups) in Fig. 4 is due to interacting shear zones between leading and trailing piles, henceforth referred to as pile ‘shadowing effects’.

Finally, Fig. 6 plots the development of the normalised maximum load deviation,  $\Delta_{\max}$ , defined as:

$$\Delta_{\max} = \frac{(N_{\max} - N_{\min})}{N_s} \quad (1)$$

where  $N_{\max}$  and  $N_{\min}$  are the maximum and minimum reaction forces among all individual piles within each group (respectively) normalised by  $s_u D$ . For both  $\alpha = 0$  and  $\alpha = 1$ , the load deviation is less for circular groups compared to square, particularly at small  $s/D$ . This agrees with the soil yielding patterns observed in Fig. 5 which shows that the rigid body of soil is fully encapsulated by the circular group unlike the square group. Interestingly, the trends for the circular groups exhibit a distinct maximum at  $s/D = 2$  and 3 for  $\alpha = 0$  and 1 (respectively) arising from a transition in the failure mechanisms from (a) block failure, where the piles are evenly distributed around the periphery of the rigid soil block (in contrast to the square group which has piles located *within* the block), through to (b) local interactions, where shadowing effects have a detrimental influence on group capacity. For square groups, there are subtle trade-offs in the transition between block failure and local failure. At low  $s/D$ , shearing

occurs at the pile-soil interface at the side of the group for  $\alpha = 0$ ; this leads to increased non-uniformity in the load-sharing compared to the  $\alpha = 1$  case where shearing occurs in the surrounding soil and the piles are fully encapsulated by the rigid block. Slight increases in  $\Delta_{\max}$  are also evident for an increase in  $n$  and reduction in  $\alpha$ .

### *Influence of load direction*

The influence of the load direction,  $\theta$ , on the normalised capacity is investigated in Fig. 7. The results show that, for all values of  $s/D$ , minimal variations in  $N_g$  occur with  $\theta$  for square groups with  $n = 8$ ; minor differences are only notable for closely spaced rough piles. Similarly, there is no effect of  $\theta$  on  $N_g$  for circular groups due to multiple symmetry axes. Soil failure in this region is dominated by the width of the rigid soil body encapsulated within the group and, thus, the load direction plays a secondary role on the lateral capacity.

## **EFFICIENCY COMPARISONS BETWEEN PERIMETER AND FULL PILE GROUPS**

In a realistic design scenario, it is common to undertake a preliminary foundation assessment to identify an approximate number of piles based on single pile values and subsequently ‘knock down’ the capacity using appropriate  $p$ -multipliers or efficiency factors. To this end, present calculations of the capacity factor  $N_g$  for square and circular groups are compared with those documented in Sheil (2021) for full square groups to quantify the impact of relocating inner piles to the periphery of the group. The results of this exercise are presented in Fig. 8 for a fixed value of  $n = 16$ .

For the given  $n$ , the lateral capacity of the perimeter groups is greater than for the full groups when  $s/D \leq 2$  and 3 for  $\alpha = 0$  and 1 respectively. This is due to the greater plan area  $A$



(dominating the block failure mechanism for closely spaced piles) comprised within the external piles for the perimeter groups compared to the more compact full group. Conversely,  $N_g$  for a full group is higher than the perimeter groups for intermediate spacings.

To extend these trends across different group sizes, similar comparisons are made in Fig. 9, this time plotted as a function of  $n$ . For  $\alpha = 0$ , there is good agreement between the three group configurations for small  $n$  (see Fig. 9(a)). As  $n$  increases, this agreement deteriorates, and the perimeter groups now exhibit greater and lower capacities relative to full groups for low and high  $s/D$ , respectively. In contrast, an increase in  $\alpha$  to 1 causes a relative improvement in the perimeter group capacity, particularly for large groups of closely spaced piles. These results suggest that for practical pile spacings ( $s/D \gtrsim 2$ ), perimeter groups do not necessarily increase capacity efficiency over standard group arrangements, particularly if the piles are smooth.

Swallow and Sheil (2021) showed that pile interaction effects were dominated by the number of group columns ( $n_c$ ; parallel to direction of loading). Reduced values of  $N_g$  for the perimeter groups observed in Figs. 8 and 9 are therefore attributable to a greater  $n_c$  compared to a full group for the same  $n$ . The influence of  $n_c$  on the development of group capacity with  $s/D$  for a square perimeter and full pile group is presented in Fig. 10 considering both  $N_g$  (Figs. 10(a)) and the total normalised group reaction,  $nN_g$  (Figs. 10(b)); thus these analyses deal with the situation where there may be a limited plan area for the foundation such that the aim is to maximise the group efficiency whilst meeting capacity requirements. From Fig. 10(a), there is reasonable agreement between the two group configurations for  $n_c = 3$ . However, an increase in  $n_c$  leads to significant reductions in  $N_g$  for the full groups compared to the perimeter groups. This is because the internal group piles are located within the block failure mechanism and therefore contribute little to the lateral capacity for low values of  $s/D$ . This is shown in Fig. 10(b) where the same values of  $nN_g$  are achieved for both the perimeter and full

groups for closely spaced piles ( $s/D < 1.5$ ). For  $s/D > 1.5$ , soil failure is no longer dominated by  $A$  and full groups show greater values of  $nN_g$ .

## CONCLUSIONS

This paper has described a finite element study of the deep soil failure mechanisms associated with laterally loaded perimeter pile groups embedded in undrained soil. For practical pile spacings (two to six pile diameters), the numerical results shows that square groups exhibit a hybrid mechanism comprising global flow-around and local interactions between piles, whereas circular groups exhibit local interactions only. When compared to ‘full’ square pile groups with the same number of piles, perimeter groups did not necessarily increase capacity efficiency for spacings less than two pile diameters, particularly if the piles are smooth. Nevertheless, this paper identifies desirable features of circular perimeter groups compared to traditional full square groups: (a) the (albeit slight) improvement in the invariance of their capacity to the direction of loading and (b) the more uniform load-sharing between piles.

## ACKNOWLEDGEMENTS

The last author is supported by the Royal Academy of Engineering under the Research Fellowship scheme.

## REFERENCES

- AASHTO, L. (2012) AASHTO LRFD bridge design specifications.
- Brown, D.A., Reese, L.C. and O’Neill, M.W., 1987. Cyclic lateral loading of a large-scale pile group. *Journal of Geotechnical Engineering*, 113(11): 1326–1343.
- Brown, D.A. and Shie, C.F. 1991. Some numerical experiments with a three dimensional finite element model of a laterally loaded pile. *Computers and Geotechnics*, 12(2): 149–162.

209 Comodromos, E.M and Pitilakis K. 2005. Response Evaluation of Horizontally Loaded  
210 Fixed-Head Pile Groups using 3-D Nonlinear Analysis, *International Journal for*  
211 *Numerical and Analytical Methods in Geomechanics*, 29(6): 597-625.

212 Comodromos E.M. and Papadopoulou M.C. 2012. On the response prediction of laterally  
213 loaded pile groups in clayey soils. *Géotechnique*, 62(4): 329–339.

214 Comodromos E.M. and Papadopoulou M.C. 2013. Explicit extension of the p-y method to  
215 pile groups in cohesive soils, *Computers & Geotechnics*, 47: 28-41.

216 Dash, S., Rouholamin, M., Lombardi, D. and Bhattacharya, S., 2017. A practical method for  
217 construction of py curves for liquefiable soils. *Soil Dynamics and Earthquake*  
218 *Engineering*, 97: 478-481.

219 Fayyazi, M.S., Taiebat, M. and Liam Finn, W.D. 2014. Group reduction factors for analysis  
220 of laterally loaded pile groups. *Canadian Geotechnical Journal*, 51(7): 758-769.

221 FEMA, 2012. “Foundation analysis and design”, FEMA P–751, Washington, DC.

222 Georgiadis, K., Sloan, S.W. and Lyamin, A.V., 2013a. Effect of loading direction on the  
223 ultimate lateral soil pressure of two piles in clay. *Géotechnique*, 63(13): 1170.

224 Georgiadis, K., Sloan, S.W. and Lyamin, A.V., 2013b. Ultimate lateral pressure of two  
225 side-by-side piles in clay. *Géotechnique*, 63(9): 733.

226 Ilyas, T., Leung, C.F., Chow, Y.K. and Budi, S.S. 2004. Centrifuge model study of laterally  
227 loaded pile groups in clay. *Journal of Geotechnical and Geoenvironmental*  
228 *Engineering*, 130(3): 274-283.

229 Kallehave, D., Thilsted, C.L. and Liingaard, M.A., 2012, January. Modification of the API py  
230 formulation of initial stiffness of sand. In *Offshore site investigation and geotechnics:*  
231 *integrated technologies-present and future*. Society of Underwater Technology.

232 Kong, D., 2015. *Large displacement numerical analysis of offshore pipe-soil interaction on*  
233 *clay* (Doctoral dissertation, University of Oxford).

234 Liu, X., Cai, G., Liu, L., Liu, S., Duan, W. and Puppala, A.J., 2021. Improved py curve  
235 models for large diameter and super-long cast-in-place piles using piezocone  
236 penetration test data. *Computers and Geotechnics*, 130: 103911.

237 Mandolini, A. and Viggiani, C., 1997. Settlement of piled foundations. *Géotechnique*, 47(4),  
238 pp.791-816.

239 Martin, C.M., 2011. The use of adaptive finite-element limit analysis to reveal slip-line fields.  
240 *Géotechnique Lett.* 1: 23–29. <https://doi.org/10.1680/geolett.11.00018>.

241 Martin, C.M. and Randolph, M.F., 2006. Upper-bound analysis of lateral pile capacity in  
242 cohesive soil. *Géotechnique*, 56(2): 141-145.

243 McCabe, B.A. and Sheil, B.B., 2015. Pile group settlement estimation: suitability of  
244 nonlinear interaction factors. *International Journal of Geomechanics*, 15(3): 04014056.

245 Murff, J.D. and Hamilton, J.M., 1993. P–ultimate for undrained analysis of laterally loaded  
246 piles. *Journal of Geotechnical Engineering*, 119(1): 91–107.

247 Randolph, M.F. and Houlsby, G.T., 1984. The limiting pressure on a circular pile loaded  
248 laterally in cohesive soil. *Géotechnique*, 34(4): 613–623.

249 Rao, S.N., Ramakrishna, V.G.S.T. and Rao, M.B., 1998. Influence of rigidity on laterally  
250 loaded pile groups in marine clay. *Journal of Geotechnical and Geoenvironmental*  
251 *Engineering*, 124(6), pp.542-549.

252 Rollins, K.M., Olsen, K.G., Jensen, D.H., Garrett, B.H., Olsen, R.J. and Egbert, J.J., 2006.  
253 Pile spacing effects on lateral pile group behaviour: Analysis. *Journal of Geotechnical*  
254 *and Geoenvironmental Engineering*, 132(10): 1272–1283.

255 Shewchuk, J.R., 2002. Delaunay refinement algorithms for triangular mesh generation.  
256 *Comput. Geom.* 22: 21–74. [https://doi.org/10.1016/S0925-7721\(01\)00047-5](https://doi.org/10.1016/S0925-7721(01)00047-5)

257 Shewchuk, J.R., 1996. Triangle: Engineering a 2D quality mesh generator and Delaunay  
258 triangulator, in: *Applied Computational Geometry: Towards Geometric Engineering*,  
259 *Lecture Notes in Computer Science*. Presented at the Workshop on Applied  
260 *Computational Geometry*, pp. 203–222. <https://doi.org/10.1007/BFb0014497>.

261 Sheil, B.B., 2021. Lateral limiting pressure on square pile groups in undrained  
262 soil. *Géotechnique*, 71(4), pp.279-287.

263 Sheil, B.B. and McCabe, B.A., 2014. A finite element–based approach for predictions of  
264 rigid pile group stiffness efficiency in clays. *Acta Geotechnica*, 9(3): 469-484.

265 Sheil, B.B. and McCabe, B.A., 2015. Numerical modelling of pile foundation angular  
266 distortion. *Soils and Foundations*, 55(3), pp.614–625.

267 Sheil, B.B., McCabe, B.A., Comodromos, E.M. and Lehane, B.M., 2019. Pile groups under  
268 axial loading: an appraisal of simplified non-linear prediction  
269 models. *Géotechnique*, 69(7): 565-579.

270 Swallow, A. and Sheil, B., 2021. Group shape effects on the lateral capacity of pile groups in  
271 undrained soil. *Géotechnique*. In press.

272 Wang, A.D., Wang, W.D., Huang, M.S., Wu, J.B., Sheil, B.B. and McCabe, B.A., 2016.  
273 Discussion: Interaction factor for large pile groups. *Géotechnique Letters*, 6(3): 234-  
274 240.

275 Yao, W., Liu, Y. and Chen, J., 2012. Characteristics of negative skin friction for superlong  
276 piles under surcharge loading. *International Journal of Geomechanics*, 12(2): 90-97.

277 Zhang, Y. and Andersen, K.H., 2017. Scaling of lateral pile py response in clay from  
278 laboratory stress-strain curves. *Marine Structures*, 53, pp.124-135.

279 Zhao, Z., Kouretzis, G., Sloan, S. and Gao, Y., 2017a. Ultimate lateral resistance of tripod  
280 pile foundation in clay. *Computers and Geotechnics*, 92: 220–228.

281 Zhao, Z., Li, D., Zhang, F. and Qiu, Y., 2017b. Ultimate lateral bearing capacity of tetrapod  
282 jacket foundation in clay. *Computers and Geotechnics*, 84: 164–173.

**Table 1** Pile/soil parameters considered in the present FE modelling. \*Loading angles were chosen to achieve greatest deviation considering various axes of symmetry

Parameter	Values
Group size, $n$	8, 12, 16
Normalised pile spacing, $s/D$	1.05, 1.5, 2, 3, 4, 5, 6, 7
Pile roughness factor, $\alpha$	0, 1
Group shape	Square, circular
Direction of loading, $\theta^*$	0, $\pi/4$ (square) or 0, $\pi/8$ (circular)

**Table 2** Comparison between present FE calculations of  $N_s$  and those documented in Randolph and Houlsby (1984) and Martin and Randolph (2006)

Pile roughness factor, $\alpha$	Present FE: $N_s$	Randolph & Houlsby (1984): $N_s$ (% error)	Martin & Randolph (2006): $N_s$ (% error)
0	9.25	9.14 (1.19%)	9.20 (0.54%)
1	12.12	11.94 (1.49%)	11.94 (1.49%)

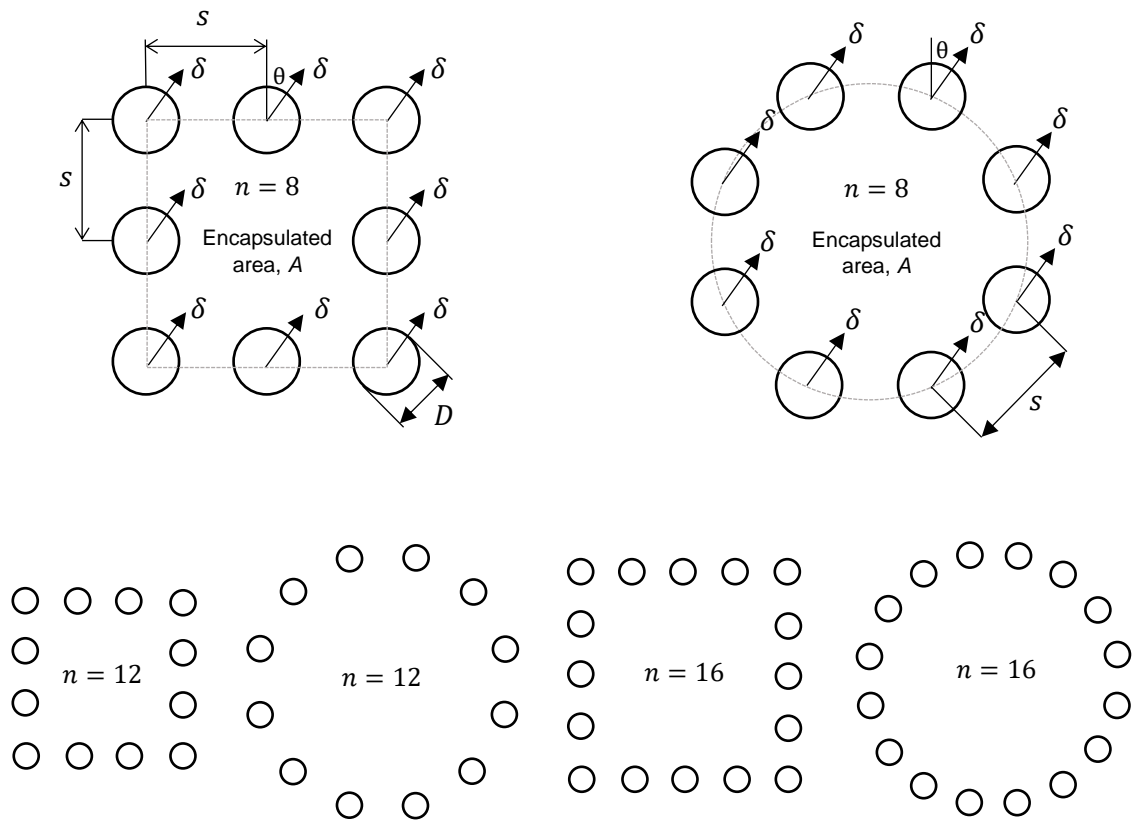


**Fig. 1** Problem definition showing perimeter group geometries and default orientations.

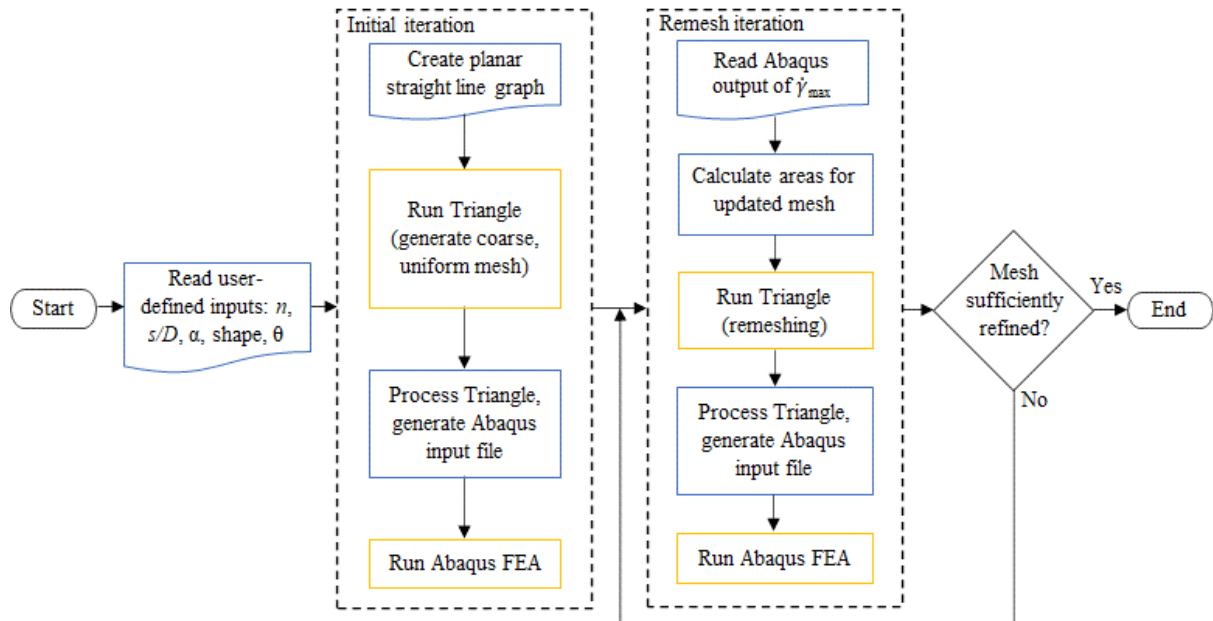


**Fig. 2** Overview of the developed adaptive remeshing FE procedure.

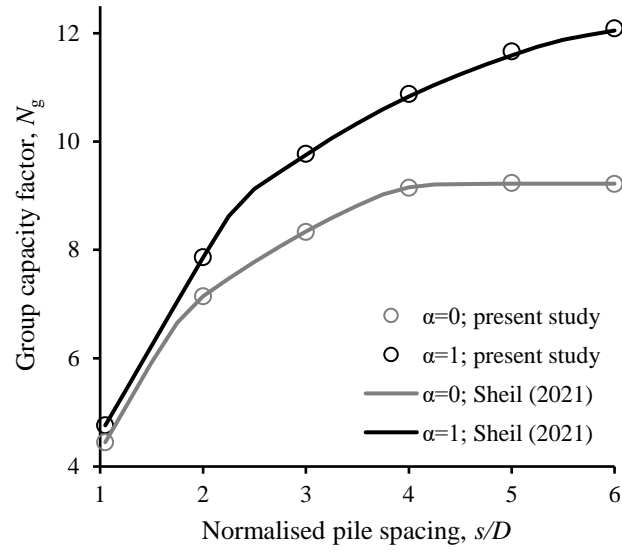


**Fig. 3** Comparison between present FE calculations of  $N_g$  and those documented in Sheil (2021) plotted as a function of  $s/D$  for a ‘full’  $3 \times 3$  square pile group and values of  $\alpha$  of 0 and 1;  $\theta = 0$ .



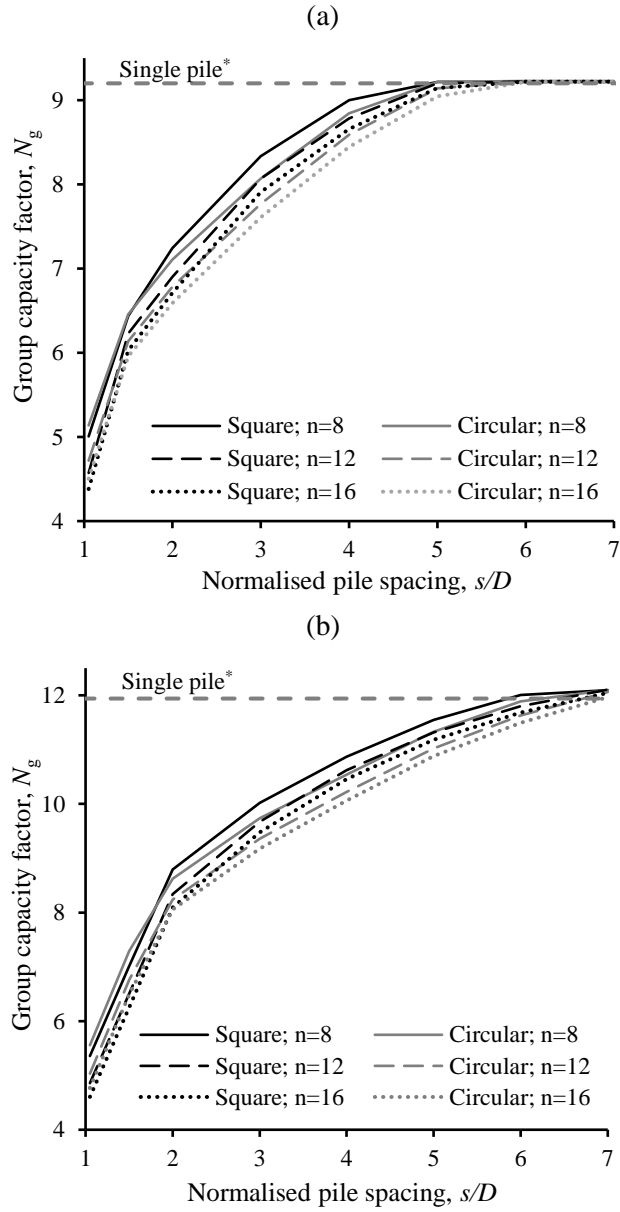


**Fig. 4** FE calculations of the influence of  $n$  and  $s/D$  on  $N_g$  for both a square and circular perimeter pile group: (a)  $\alpha = 0$ , (b)  $\alpha = 1$ ;  $\theta = 0$ . \*Single pile solutions taken from Martin & Randolph (2006). The slight over-prediction of single pile values at high  $s/D$  is attributable to numerical error (associated with level of mesh refinement) which was  $<1.5\%$  in all cases.

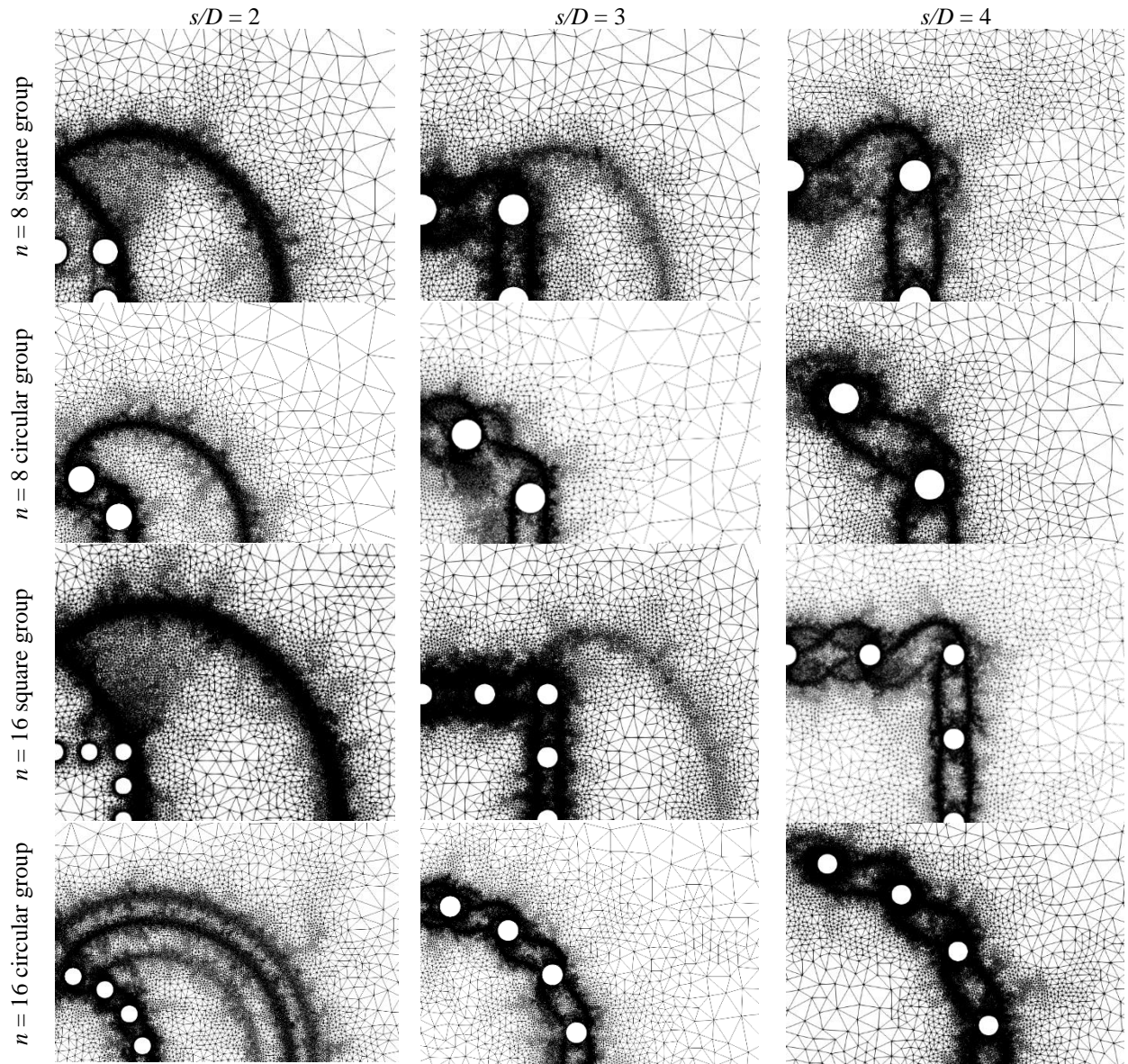
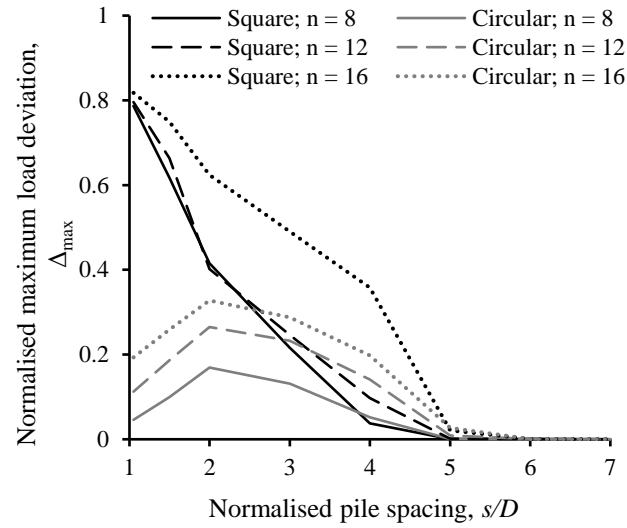


**Fig. 5** Refined FE meshes revealing soil failure mechanisms for an  $n = 8$  and  $n = 16$  perimeter pile group considering influence of pile spacing and group configuration (note only upper right-hand quadrant of mechanism shown due to symmetry);  $\alpha = 0$ ,  $\theta = 0$ .



(b)

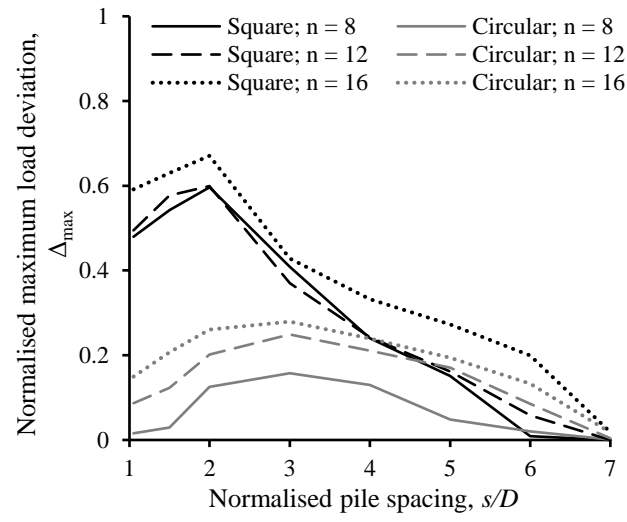


**Fig. 6** FE calculations of the influence of  $n$  and  $s/D$  on the normalised maximum load deviation  $\Delta_{\max}$

for both a square and circular perimeter pile group: (a)  $\alpha = 0$ , (b)  $\alpha = 1$ ;  $\theta = 0$ .

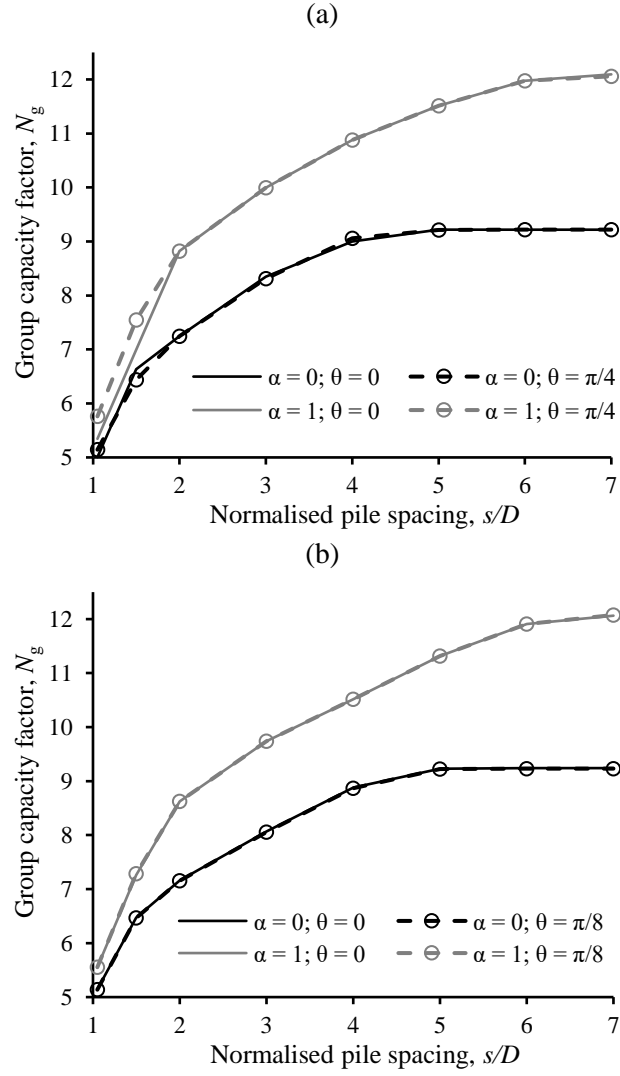


**Fig. 7** FE calculations of the influence of load direction,  $\theta$ , on the variation of  $N_g$  with  $s/D$  considering values of  $\alpha$  of 0 and 1: (a) square perimeter group, (b) circular perimeter group.

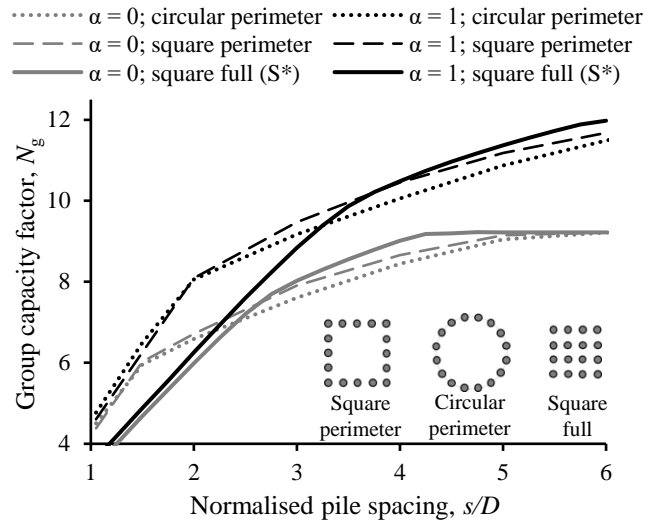


**Fig. 8** FE calculations of the influence of group configuration on the development of  $N_g$  with  $s/D$  for a fixed group size of  $n = 16$ ;  $\theta = 0$ . \*S = Sheil (2021).

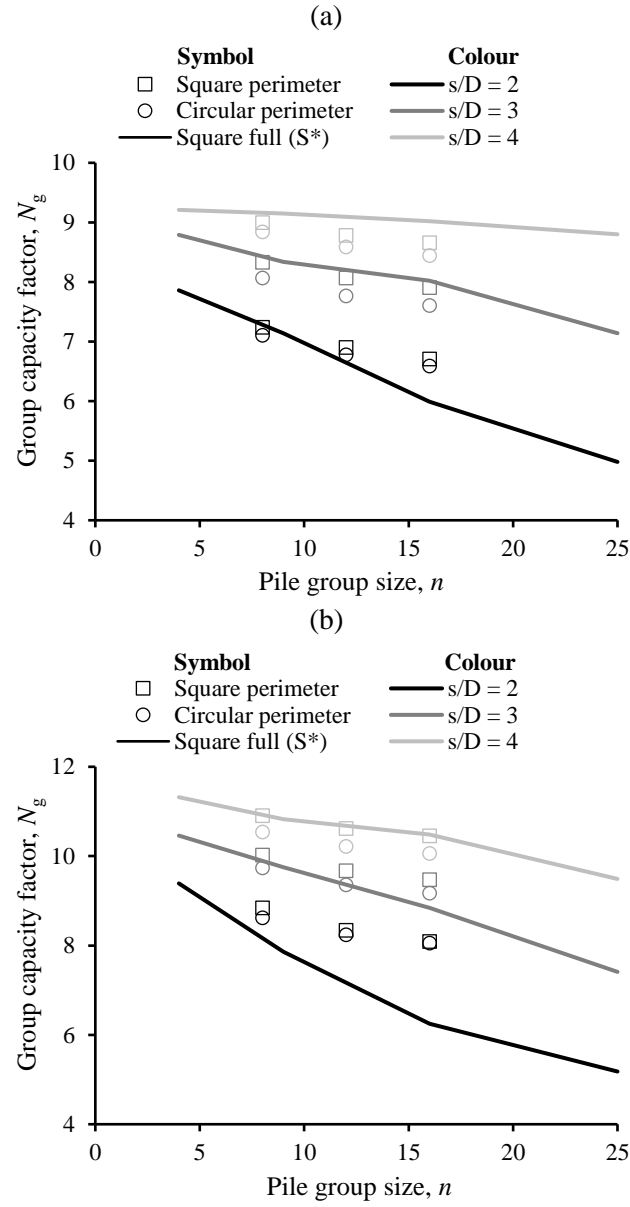


**Fig. 9** FE calculations of the influence of group configuration on the development of  $N_g$  with group size: (a)  $\alpha = 0$ , (b)  $\alpha = 1$ ;  $\theta = 0$ . \*S = Sheil (2021).

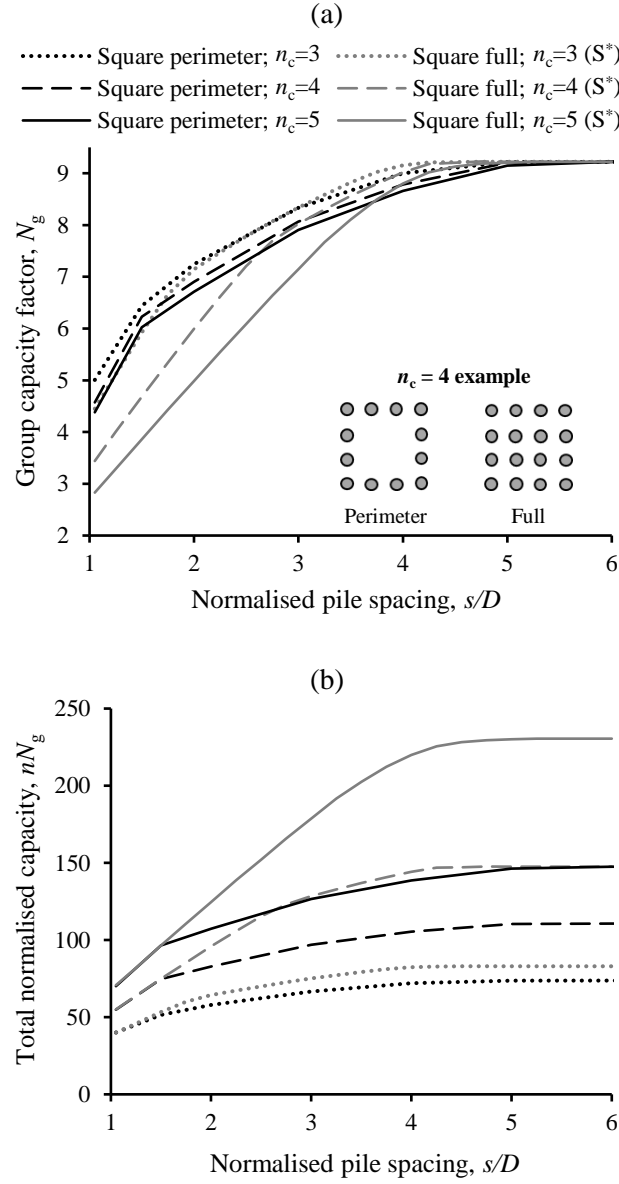


**Fig. 10** Group capacity comparisons between square perimeter and full pile groups for the same maximum number of pile columns,  $n_c$ : (a) group capacity factor  $N_g$  and (b) total normalised capacity

$nN_g$ ;  $\alpha = 0$ ,  $\theta = 0$ . \*S = Sheil (2021).